

Tightly self-trapped modes and vortices in three-dimensional bosonic condensates with the electromagnetically-induced gravity

Zibin Zhao^{1,*}, Guilong Li^{1,*}, Huanbo Luo^{1,2,†}, Bin Liu^{1,3}, Gui-hua Chen^{4,‡}, Boris A. Malomed^{5,6}, and Yongyao Li^{1,3}

¹*School of Physics and Optoelectronic Engineering, Foshan University, Foshan 528000, China*

²*Department of Physics, South China University of Technology, Guangzhou 510640, China*

³*Guangdong-Hong Kong-Macao Joint Laboratory for Intelligent Micro-Nano Optoelectronic Technology, Foshan University, Foshan 528225, China*

⁴*School of Electronic Engineering & Intelligentization, Dongguan University of Technology, Dongguan 523808, China*

⁵*Department of Physical Electronics, School of Electrical Engineering, Faculty of Engineering, Tel Aviv University, Tel Aviv 69978, Israel*

⁶*Instituto de Alta Investigación, Universidad de Tarapacá, Casilla 7D, Arica, Chile*

The $1/r$ long-range interaction, induced by laser illumination, offers a mechanism for the implementation of stable self-trapping in Bose-Einstein condensates (BECs) in the three-dimensional free space. Using the variational approximation and numerical solutions, we find that self-trapped states in this setting, with attractive nonlocal and repulsive local interactions, resemble tightly-bound compactons. However, these are not true compactons but rather *tightly self-trapped modes* (TSTMs), with small-amplitude nonvanishing tails. The structure of the self-trapped states is explained by an analytical solution for their tails. Further, we demonstrate that stable TSTMs with embedded vorticity, exist in the same setting, with winding numbers up to $S = 6$ (at least). Addressing two-TSTM interactions, we find that pairs of ground states (GSs, with $S = 0$), as well as vortex-vortex and vortex-antivortex pairs (with $S_1 = S_2$ and $S_1 = -S_2$, respectively), form stably rotating bound states. Head-on collisions between vortex TSTMs, set in slow motion by kicks, are inelastic, resulting in their merger into a GS soliton, that may either remain at the collision position or move aside, shedding the angular momentum with emitted radiation, or, alternatively, lead to the formation of a vortex that also moves aside.

I. INTRODUCTION

In the realm of nonlinear physics, solitons are known for their unique stability and propagation characteristics [1–6]. Solitons exist in a great variety of models [7–25], where they typically exhibit exponentially decaying tails. As a class of tailless self-trapped states with a compact support, Rosenau and Hyman (1993) introduced the concept of compactons [26], which are produced by real nonlinear equations. A typical structure of the compacton solution is

$$u(r) = \begin{cases} A \cos^2(\pi r/D) H_s(D/2 - r), & \text{at } r < D/2, \\ 0, & \text{at } r > D/2, \end{cases} \quad (1)$$

where r is the radial coordinate, H_s is the Heaviside step-function, while A and D denote the amplitude and diameter of the spatially confined mode [27].

Compactons are also known as solutions of specially designed discrete models [28, 29]. In particular, stable single- and multisite discrete compactons can be maintained by the combination of a deep optical lattice and fast time-periodic modulation of the nonlinearity [30]. However, compacton-like modes have not been previously predicted in continuous three-dimensional (3D) BEC sys-

tems (without the use of deep optical lattices). The objective of the present work is to establish stable tightly self-trapped modes (TSTMs) as natural ground and excited (vortical) states in a BEC with specific long-range inter-atomic interactions.

It is well known that long-range interactions offer a wide range of possibilities for the creation of spatial modes in BEC. Common types of such interactions are represented by dipole-dipole forces, which have been studied in detail theoretically and experimentally [31–39], and soft-core phenomena. Anisotropic dipole-dipole interactions, with the interatomic potential $\sim 1/r^3$, occur in BECs of atoms with large magnetic moments. Soft-core interactions, on the other hand, arise from the coupling between Rydberg and ground atomic states, with widely tunable strengths [40–44]. Unlike hard-core interactions, where the potential becomes infinite at short distances, the soft-core potential saturate to a finite value as the atoms approach each other. These two types of long-range interactions not only support the formation of self-trapped 3D states, but also enable the emergence of novel quantum states of matter, such as supersolids [45–53].

In addition to these settings, it was proposed by O’Dell et al. [54] to induce an atomic interaction with an attractive potential similar to the gravitational one, scaling as $-1/r$, by means of a set of six suitably arranged far-off-resonant laser beams. An estimate demonstrates that this interaction may be stronger than the proper gravitational attraction between the same atoms by $\simeq 17$ orders of magnitude, offering an efficient method to simu-

* These authors contributed equally to this work.

† huanboluo@fosu.edu.cn

‡ cghphys@gmail.com

late quasi-gravitational effects in quantum systems, such as the realization of self-trapping in the free space [55–57], or investigate quantum nonlinear phenomena in the number-conserving analogues of gravity within BEC [58].

For the analysis of ground and excited states in BEC with long-range interactions, an extended variational approximation (VA) was elaborated, based on an ansatz in the form of a sum of Gaussians with a common center but different width parameters [59, 60], the commonly known VA based on the single Gaussian being the lowest-order form of this approach. The VA-predicted results become essentially more accurate (while the computational procedure becomes more cumbersome) with the increase of the number of the Gaussian terms in the ansatz.

In this paper, we develop VA for TSTMs, using a compacton ansatz, and compare the ensuing results with numerical findings, as well as with VA results produced by a simple Gaussian ansatz. We conclude that the results for the TSTMs, generated by the compacton ansatz, are essentially more accurate (closer to the numerical findings) than their Gaussian-based counterparts. In addition to the ground state (GS) of TSTMs, the analysis reveals stable TSTMs with embedded vorticity. It is well known that, in other models admitting vortex solitons, those carrying high topological charges are usually unstable in the free space against azimuthal perturbations, which break the vortices into fragments or lead to their decay into GS [25, 61]. In the present situation, we find that the gravity-like self-attraction stabilize vortex states with topological charges up to (at least) $S = 6$. The fact that the long-range attraction with the potential $\sim -1/r$ can support stable vortex modes (in particular, ones with high values of S) has not been reported previously. In this connection, it is relevant to stress that, while many mechanisms were proposed for the stabilization of vortex solitons, the stability remains a challenging issue for $S > 1$, especially in the 3D space [62–77].

The following material is organized as follows. The 3D model with the gravity-like self-attraction is introduced in Section 2. In that section, we also produce an analytical solution for the TSTMs' asymptotic tails. It demonstrates that the edge of the self-trapped state becomes much sharper for the states with a sufficiently large norm, which explains the proximity of their shape to the compacton. VA for the TSTMs of the GS type (with zero vorticity) is elaborated and compared to numerical findings in Section 3. Numerical results for 3D stationary TSTMs, of both the GS and vortex types, including the test of their stability, are reported in Section 4. Further, dynamics of the GSs and vortices, including the formation of stable orbiting bound states and collisions between moving TSTMs, is investigated by means of direct simulations in Section 5. In particular, it is demonstrated that GS pairs, as well as vortex-antivortex ones, form stable configurations with mutual orbiting, while collisions result in inelastic outcomes. The paper is concluded by Section 6.

II. THE MODEL

The potential of the gravity-like inter-atomic attraction for BEC illuminated by the appropriate set of laser beams with wave vector k and intensity I was derived in Ref. [54]:

$$U(R) = -\frac{11}{4\pi} \frac{Ik^2\alpha^2}{c\epsilon_0^2} \frac{1}{R} = -\frac{K}{R}, \quad (2)$$

where c and ϵ_0 are the light speed and permittivity in the free space, $\alpha(k)$ is the isotropic dynamical polarizability of the laser, and I is the intensity of the laser, and R is the distance between the interacting atoms. The setup is designed so that the usual dipole-dipole-like term, $\sim R^{-3}$ is averaged out, while the one $\sim -R^{-1}$ does not vanish. Thus, BEC with the gravity-like attraction is governed by the Gross-Pitaevskii equation (GPE), written as

$$i\hbar \frac{\partial}{\partial T} \Psi = -\frac{\hbar^2}{2M} \nabla^2 \Psi + G|\Psi|^2 \Psi - K\Psi \int \frac{|\Psi(\mathbf{R}')|^2}{|\mathbf{R} - \mathbf{R}'|} d\mathbf{R}', \quad (3)$$

where $G = 4\pi\hbar^2 a_s/M$ is the coefficient of the contact interaction (a_s is the s -wave scattering length of atomic collisions, and M is the atomic mass). The estimate for K given in Ref. [54] for a CO₂ laser light with intensity $I = 100$ MW/cm² amounts to $-K/R \approx -2 \times 10^{-15}$ eV at $R = 100$ nm. The total number of atoms in this setup is

$$\mathcal{N} = \int |\Psi(\mathbf{R})|^2 d^3\mathbf{R}, \quad (4)$$

the set of control parameters being a_s, I and \mathcal{N} . Using the normalization

$$T = t_0 \cdot t, \quad \mathbf{R} = l_0 \cdot \mathbf{r}, \quad \Psi = l_0^{-\frac{3}{2}} \cdot \psi, \quad (5)$$

where t_0 and $l_0 = \sqrt{\hbar t_0/M}$ are time and length scales, the dimensionless GPE can be obtained as:

$$i\partial_t \psi = -\frac{1}{2} \nabla^2 \psi + g|\psi|^2 \psi - \kappa \psi \int \frac{|\psi(\mathbf{r}')|^2}{|\mathbf{r} - \mathbf{r}'|} d\mathbf{r}', \quad (6)$$

where

$$g = 4\pi a_s/l_0, \quad \kappa = K M l_0/\hbar^2 \quad (7)$$

are dimensionless strengths of the local and nonlocal interactions, respectively.

Equation (3) shares the property of the Galilean invariance with the broad class of nonlinear Schrödinger equations, which include the same linear operator. This means that the substitution of

$$\psi(\mathbf{r}, t) = \exp(i\mathbf{v} \cdot \mathbf{r} + i(v^2/2)t) \tilde{\psi}(\mathbf{r} - \mathbf{v}t, t), \quad (8)$$

with an arbitrary vectorial velocity \mathbf{v} , in Eq. (6) transforms it into the same equation, but with ψ replaced by $\tilde{\psi}$ and \mathbf{r} replaced by $\tilde{\mathbf{r}} \equiv \mathbf{r} - \mathbf{v}t$. In other words, the

Galilean transform (8) converts any solution of Eq. (6) into its counterpart moving with velocity \mathbf{v} and carrying additional phase $\mathbf{v} \cdot \mathbf{r} + (v^2/2)t$.

In fact, Eq. (6) admits additional rescaling (not used here), which makes it possible to set $g = 1$ (unless $g = 0$) and $\kappa = 1$ [78]. In the subsequent numerical studies, we refer to ^{87}Rb and select $l_0 = 0.5 \mu\text{m}$ (which corresponds to $t_0 \approx 0.03 \text{ ms}$), without using this rescaling.

It is relevant to mention that Eq. (6) belongs to the class of Schrödinger-Poisson (SP) equations, which were considered in the context of various physical models – in particular, cosmology [79–84]. The existence of GS solutions to SP equations in 3D was rigorously established (in particular, by means of the variational method [85–89]). Dynamics of delocalized vortices in plasmas, governed the SP system, was addressed too [90]. Vortex solitons produced by the SP and their stability against the spontaneous splitting in 2D and 3D were also studied in detail [91–97], as well as incoherent (turbulent) self-trapped states [98].

Stationary solutions to Eq. (6) with chemical potential μ are looked for as

$$\psi = \varphi(\mathbf{r}) \exp(-i\mu t), \quad (9)$$

with (generally speaking, complex) function φ obeying the stationary GPE:

$$\mu\varphi = -\frac{1}{2}\nabla^2\varphi + g|\varphi|^2\varphi - \kappa\varphi \int \frac{|\varphi(\mathbf{r}')|^2}{|\mathbf{r} - \mathbf{r}'|} d\mathbf{r}'. \quad (10)$$

The energy (Hamiltonian) of GPE (6) is

$$E = \int d\mathbf{r} \left[\frac{1}{2} |\nabla\varphi|^2 + \frac{1}{2} g |\varphi|^4 \right] - \frac{\kappa}{2} \iint \frac{d\mathbf{r} d\mathbf{r}'}{|\mathbf{r} - \mathbf{r}'|} |\varphi(\mathbf{r}')|^2 |\varphi(\mathbf{r})|^2. \quad (11)$$

It is relevant to analyze the tail of self-trapped states produced by Eq. (10) with $\mu < 0$ at $r \rightarrow \infty$. In this limit, the linearization of Eq. (10) takes the following form, in the lowest approximation:

$$\mu\varphi + \frac{1}{2} \left(\frac{d^2}{dr^2} + \frac{2}{r} \frac{d}{dr} \right) \varphi + \kappa \frac{N}{r} \varphi = 0, \quad (12)$$

where

$$N = \int |\varphi|^2 d^3\mathbf{r} \quad (13)$$

is the total norm of the self-trapped state (the same asymptotic equation (12) is relevant for the self-trapped states with embedded vorticity). A straightforward asymptotic solution of Eq. (12) is

$$\varphi = \varphi_0 r^{\kappa N / \sqrt{-2\mu} - 1} \exp\left(-\sqrt{-2\mu} r\right) \text{ at } r \rightarrow \infty, \quad (14)$$

where φ_0 is a constant (this solution is different from the commonly known ground-state wave function of the hydrogen atom, which formally corresponds to $\kappa N / \sqrt{-2\mu} -$

$1 = 0$). In the case of $N \gg \sqrt{-2\mu}/\kappa$, the gravity-like attraction draws the tail into the body of the self-trapped state, thus making the edge of the state sharper, which is the distinct feature of TSTMs. Indeed, the waveform (14) with large N has a maximum at $r_{\text{max}} \approx \kappa N / (-2\mu)$, which, roughly speaking, determines the QC's radius, while the maximum does not exist at $N < \sqrt{-2\mu}/\kappa$.

III. THE VARIATIONAL APPROXIMATION FOR THE GS (GROUND STATE)

The GS wave function φ is real, hence Eq. (10) amounts to the real one:

$$\mu\phi = -\frac{1}{2} \left(\frac{d^2}{dr^2} + \frac{2}{r} \frac{d}{dr} \right) \phi - \kappa\phi(r) \int \frac{\phi^2(\mathbf{r}')}{|\mathbf{r} - \mathbf{r}'|} d\mathbf{r}' + g\phi^3. \quad (15)$$

The Lagrangian corresponding to Eq. (15) is

$$L = \int d\mathbf{r} \left[\frac{1}{2} \left(\frac{d\phi}{dr} \right)^2 - \frac{\mu}{2} \phi^2 + \frac{g}{4} \phi^4 \right] - \frac{\kappa}{2} \iint \frac{d\mathbf{r} d\mathbf{r}'}{|\mathbf{r} - \mathbf{r}'|} \phi^2(\mathbf{r}) \phi^2(\mathbf{r}'). \quad (16)$$

Two VA *ansätze* for GS in 3D are adopted as the compacton $\phi_1(r)$ and Gaussian $\phi_2(r)$, *viz.*,

$$\phi_1(r) = \sqrt{\frac{32\pi N}{(2\pi^2 - 15) D^3}} \cos^2\left(\frac{\pi r}{D}\right) H_s\left(\frac{D}{2} - r\right), \quad (17)$$

$$\phi_2(r) = \frac{\sqrt{N}}{\pi^{4/3} \rho^{3/2}} \exp\left(-\frac{r^2}{2\rho^2}\right), \quad (18)$$

where N is the total norm (13). Substituting these *ansätze* into Lagrangian (16), the calculation can be performed analytically (in particular, it is convenient to calculate the double integral in Eq. (16) using the coordinate transformation $\mathbf{r} - \mathbf{r}' \equiv \mathbf{r}_-, \mathbf{r} + \mathbf{r}' \equiv \mathbf{r}_+$, taking into account the respective Jacobian $1/8$). The results for the compacton (C) and Gaussian (G) are

$$L_{\text{VA-C}} = -\frac{\mu}{2} N + \frac{23N}{D^2} + \frac{2gN^2}{D^3} - \frac{2N^2\kappa}{D}, \quad (19)$$

$$L_{\text{VA-G}} = -\frac{\mu}{2} N + \frac{3N}{4\rho^2} + \frac{\sqrt{2}gN^2}{16\pi^{3/2}\rho^3} - \frac{\kappa N^2}{\sqrt{2\pi}\rho}. \quad (20)$$

Then, values of variational parameters D and ρ in *ansätze* (17) and (18) are predicted by the Euler-Lagrange equations $\partial L_{\text{VA-C}}/\partial D = 0, \partial L_{\text{VA-G}}/\partial \rho = 0$:

$$8\kappa N D^2 - 220D - 31gN = 0, \quad (21)$$

$$\kappa N \rho^2 - 4\rho - 0.1gN = 0. \quad (22)$$

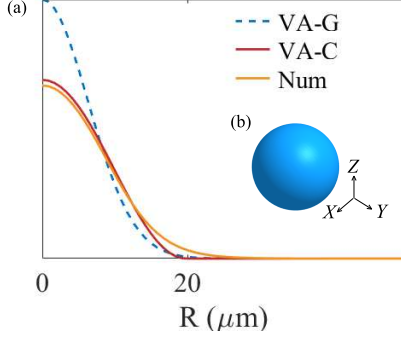


FIG. 1. A typical example of the stable GS with parameters corresponding to the condensate of 30000 atoms, with physical parameters $a_s = 100a_0$, and $I = 100 \text{ MW/cm}^2$ (a_0 is Bohr radius). The corresponding dimensionless parameters are $g = 1.33$, and $\kappa = 0.2$. (a) The blue dashed and red solid curves represent the VA prediction based, respectively, on the Gaussian and compacton *ansätze* (17) and (18), respectively. The orange solid curve is the numerical solution for the same parameters. (b) The density isosurface of the numerical solution. Direct simulation of the perturbed evolution demonstrates that the GS is stable, at least, up to $T = 100 \text{ ms}$ (corresponding to the dimensionless time $t \approx 3000$).

In the case of the local self-repulsion, $g > 0$ in Eq. (6), each equation (21) and (22) produces a single physically relevant root:

$$D = \frac{220 + \sqrt{979\kappa g N^2 + 48523}}{16\kappa N}, \quad (23)$$

$$\rho = \frac{3\sqrt{\pi}}{2\sqrt{2\kappa}N} + \sqrt{\frac{9\pi}{8\kappa^2 N^2} + \frac{3g}{8\pi\kappa}}. \quad (24)$$

Thus, once N , κ , and g are fixed, the solution's width (D for the compacton and ρ for the Gaussian) is predicted by the VA, which subsequently defines their amplitudes, as per Eqs. (17) and (18), respectively:

$$\begin{aligned} A_{\text{compacton}} &= \sqrt{32\pi N / (2\pi^2 - 15)} D^{-3/2}, \\ A_{\text{Gaussian}} &= \sqrt{N\pi}^{-4/3} \rho^{-3/2}. \end{aligned} \quad (25)$$

IV. STATIONARY SOLUTIONS

A. The ground state (GS)

To explore characteristics of GS supported by the equation (6) of the SP type, we compare the VA-predicted solutions $\phi_1(r)$ and $\phi_2(r)$ (the compacton and Gaussian approximations, respectively) with a numerical solution $\phi(r)$ of Eq. (15) for the same parameters, κ , g , and N . The latter solution was obtained as the GS of Eq. (6) using the imaginary-time method [99], with the input

$$\phi(r) = r^{|S|} \exp(-r^2/C + iS\theta), \quad (26)$$

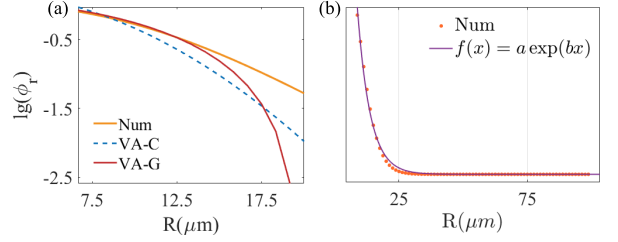


FIG. 2. Tail fitting: (a) displays the differences among the three wave functions shown in Fig. 1 within the range $R = 7.5 \sim 17.5 \mu\text{m}$. The vertical axis is plotted on a logarithmic scale, denoted as $\log_{10}(\phi) = \lg(\phi)$, where ϕ represents the corresponding wave function. Consistent with Fig. 1, the orange curve denotes the numerical solution, the blue curve corresponds to the variational solution based on the Gaussian ansatz, and the red curve represents the variational solution based on the compacton ansatz. (b) shows a fitting of the numerical solution. The orange dots represent the numerical result, while the purple curve is the fitted function. Here, we adopt an exponential decay fitting of the form $f(x) = a \exp(bx)$. In this case, the fitted parameters are $a = 2.881$ and $b = -0.8895$.

where $C > 0$ is a constant, $r = \sqrt{x^2 + y^2 + z^2}$, $\theta = \arctan(y/x)$, and $S = 0, 1, 2, \dots$ is the vorticity. The results, shown in Fig. 1 (a), indicate that the compacton ansatz provides a much better fit to the numerical solution. Figure 1(b) displays its isotropic shape in the 3D space. Stability of the GSs was tested by direct simulations of their perturbed evolution (not shown here in detail), confirming that all GSs are stable modes, as it might be expected.

Nevertheless, the GS is not a genuine compacton. As shown in Fig. 2(a), although the GS agrees well with the compacton solution in the central region, its tail does not exhibit the same rapid decay characteristic of compactons. In Fig. 2(b), we fit the tail of the GS and find that it follows an exponential decay profile. Moreover, the decay rate is found to depend on the control parameter.

To better illustrate the proximity of the self-trapped states to compactons, we compare the radius

$$r = \sqrt{\langle r^2 \rangle}, \quad \langle r^2 \rangle \equiv \int r^2 d\mathbf{r} |\varphi(\mathbf{r})|^2, \quad (27)$$

amplitudes (25), chemical potential μ and energy (11) of the Gaussian (VA), compacton (VA), and numerical solutions. In Fig. 3 (a1-a4) and (b1-b4), it is shown that the radius, amplitude and chemical potential of the VA compacton are very close to their counterparts for the numerical solution, while the Gaussian demonstrates an essential discrepancy. This is consistent with the results shown in Fig. 1. The results presented in Fig. 3 indicate that, in terms of width, amplitude, chemical potential and energy, the VA compactons are indeed very close to the numerical solutions. Further, Fig. 3 (a1-a4) demonstrates that there exists a minimum (threshold) value

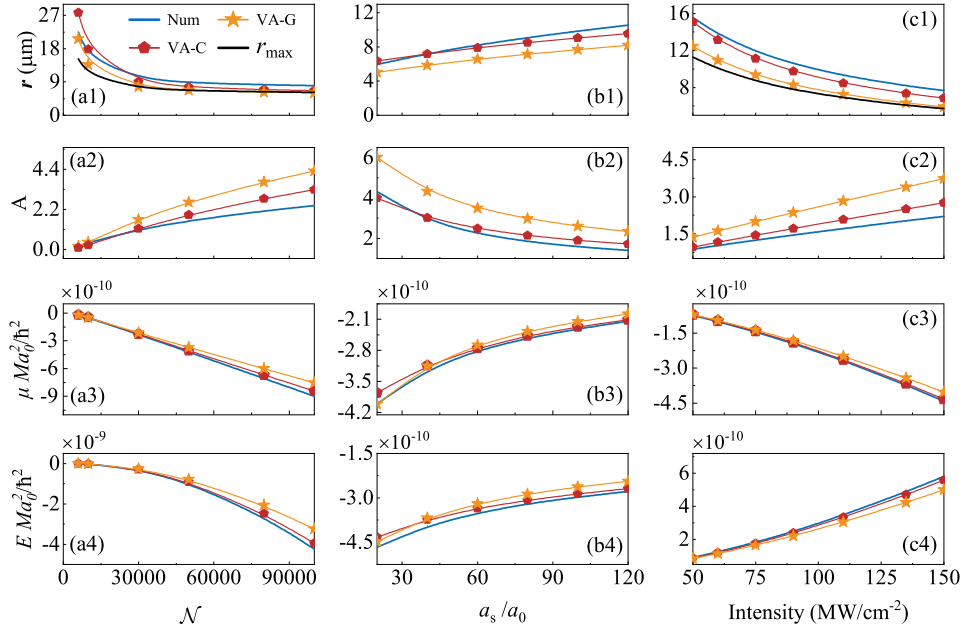


FIG. 3. Radius r (see Eq. (27)), amplitude A (see Eq. (25)), chemical potential μ (see Eq. (9)) and energy E (see Eq. (11)) vs. the number of atoms \mathcal{N} in the TSTMs (a1-a4), scattering length a_s (b1-b4), and intensity of the laser illumination (c1-c4). The blue solid curves, chains of red pentagons, and orange five-pointed stars represent the numerical results and VA predictions based on the compacton and Gaussian ansätze, respectively. The black solid lines in (a1) and (c1) represent the value of $r_{\max} \approx \kappa N / (-2\mu)$. In (a1-a4), we fix $a_s = 100a_0$ and $I = 100 \text{ MW/cm}^2$ (corresponding to $g = 1.33$ and $\kappa = 0.2$). In (b1-b4), $\mathcal{N} = 30000$ and $I = 100 \text{ MW/cm}^2$ are kept constant. In (c1-c4), the parameters are fixed as $\mathcal{N} = 30000$ and $a_s = 100a_0$.

of \mathcal{N} , below which (at $\mathcal{N} < 6000$, in this figure), self-trapped states cannot be formed. Fig. 3 (c1-c4) indicate that, as the nonlocal interaction strength, determined by the illumination intensity, increases, the discrepancy between the VA Gaussian solution and the numerical one becomes more evident, whereas the VA compacton solution consistently remains in close agreement with the numerical results, in line with the above conclusion.

In addition, we compared r_{\max} with the radius of the numerical solution in Fig. 2 (a1) and (c1). From these two figures, it can be observed that when N and κ are relatively small, there is a significant difference between r_{\max} and the actual radius of the TSTM. However, as N and κ gradually increase, particularly with an increase in N , the difference between r_{\max} and the radius of the TSTM decreases. Thus, it can be inferred that, once N is sufficiently large, the radius of the TSTM becomes close to the predicted value r_{\max} . This result is consistent with the above asymptotic analysis of self-trapped states, indicating that when N is sufficiently large, the gravitational interactions will cause the self-trapped state to exhibit a sharper tail, leading it to form as a TSTM.

In our system, TSTMs emerge as a result of the intricate balance between the gradient term (alias the kinetic energy term) and the interaction terms, which include both local and nonlocal interactions. To further illustrate this point, we consider in Fig. 4 a loosely bound mode, given by $\phi = A \exp(-R^2/(2\sigma^2))$ with $R = \sqrt{X^2 + Y^2 + Z^2}$ and a large width $\sigma = 60 \mu\text{m}$, as

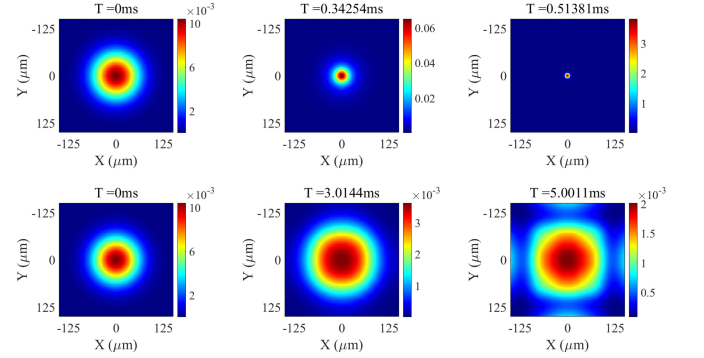


FIG. 4. The top row displays the evolution of a loosely bound input into a tightly bound state. The bottom row demonstrates that, in the absence of long-range gravity-like interaction, the same input just spreads out (at the late stage of the evolution, the isotropy of the expanding pattern is broken by proximity to the domain's boundary). For this figure, the parameters are chosen as: the total number of particles $\mathcal{N} = 100000$, the interaction strength $g = 1.33$, and the long-range interaction strength $\kappa = 0.2$ and $\kappa = 0$, in the top and bottom rows, respectively.

an input for the evolution governed by Eq. (6). Numerical simulations reveal that this initial loosely bound mode rapidly self-traps into a tightly bound state, which

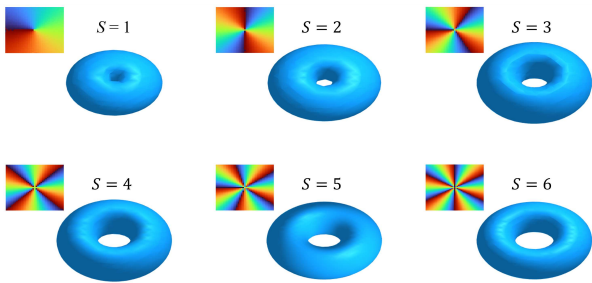


FIG. 5. Density isosurfaces of stable vortices with topological charges $S = 1 \sim 3$ and $S = 4 \sim 6$ are plotted in the first and second rows, respectively. The physical parameters are set as $a_s = 100a_0$, $I = 100$ MW/cm² and $\mathcal{N} = 370000$ ($S = 1$), 400000 ($S = 2$), 435000 ($S = 3$), 470000 ($S = 4$), 500000 ($S = 5$), 540000 ($S = 6$). In the upper left corner of each density isosurface, the phase of the wave function is shown in the $z = 0$ cross-section.

remains stable over an extended period (at least up to $T = 70$ ms in physical units), exhibiting only minor intrinsic oscillations. These results provide clear evidence for the experimental realization of tightly bound states and further confirm their robustness. Notably, if the $\sim 1/R$ nonlocal interaction term is removed from Eq. (6), the system fails to generate any tightly bound state. This highlights the crucial role of the long-range gravity-like interaction in supporting both the formation and stability of the tightly bound states.

It is worth noting that a compacton-type solution was obtained in Ref. [54], using the Thomas-Fermi (TF) approximation, given by

$$\Psi_{\text{TF-G}}(R) = \frac{\sqrt{\mathcal{N}}}{2R_0} \sqrt{\frac{\sin(\pi R/R_0)}{R}} H_s(R_0 - R). \quad (28)$$

Note that, in the framework of the TF approximation, all solutions are compactons by definition. The TF approximation reduces the original governing equations to algebraic relations, neglecting the kinetic-energy terms and thus leading to solutions that are nonzero only in regions where the potential and interaction terms are in balance, with strict truncation elsewhere. Consequently, solutions produced by the TF approximation always exhibit a compact support.

B. The vortex states

As mentioned above, in a majority of other models admitting vortex solitons, they are often unstable against spontaneous splitting, especially in the 3D geometry [25, 61]. Therefore, it is interesting to explore the TSTMs with embedded vorticity and their stability in the present case. Because the imaginary-time-integration method converges only to the GS solutions, we here used the Newton conjugate gradient method (NCG) [100] to

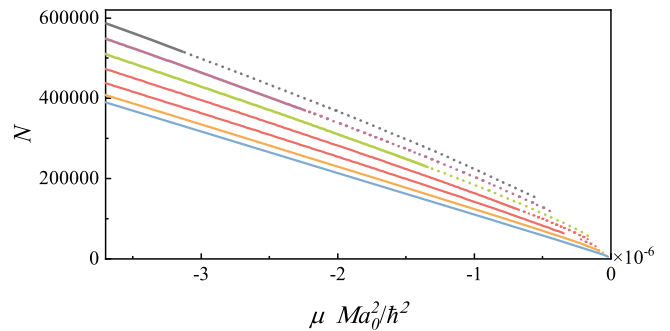


FIG. 6. The total atom number \mathcal{N} vs. chemical potential μ is shown for the GS and vortex solutions. Solid and dotted lines denote stable and unstable intervals, respectively. The curves from bottom to top pertain to topological charges $S = 0 \sim 6$, in the increasing order.

obtain vortex solutions. For the vortex solution with $S = 1$, the ansatz is given by Eq. (26) with $S = 1$. In contrast, for solutions with $S > 1$, we employ the modified ansatz

$$\phi(r) = R'^S \exp(-R'^2/C + iS\theta), \quad (29)$$

where $R' = \sqrt{(r_\perp - R_0)^2 + z^2}$, $r_\perp = \sqrt{x^2 + y^2}$, and $C > 0$, $R_0 > 0$ are constants. The modification of the ansatz for $S > 1$ is necessary because such solutions exhibit a toroidal structure with a relatively large inner radius R_0 .

Figure 5 displays density distributions in the vortex states with the topological charge from $S = 1$ to 6, and the respective phase distributions of the wave function in the $z = 0$ plane, clearly revealing the 3D toroidal structure of these solutions. The inner hole in the vortex states expands as S increases. This feature is common for vortices in continuous [101–107] and discrete [108, 109] systems. It is explained by the fact that, as S increases, the phase of the wavefunction varies more rapidly in the azimuthal direction. Therefore, a larger inner radius of the vortex is required to maintain the continuity of the wavefunction.

Stability of the vortex states was verified, as in the case of GSs, by simulations of their perturbed evolution in the framework of Eq. 6. Figure 6 summarizes the results by means of the $\mathcal{N}(\mu)$ dependences for the GS and vortex states, with solid and dotted segments indicating stable and unstable solutions, respectively. As seen from Fig. 6, when g is fixed, all vortex TSTMs remain stable for large \mathcal{N} . The same result is valid for fixed \mathcal{N} and increasing g . Thus, if g is fixed, a larger atomic number \mathcal{N} corresponds to stronger local repulsion, which favors the existence of stable vortex states. These conclusions are generally similar to those reported in other models in the two-dimensional case [110, 111]. It is seen that, as the topological charge increases, the stability interval gradually shrinks. Thus, the $1/r$ long-range interaction is beneficial for the stable existence of vortex states. As concerns the evolution of unstable vortex states, it is displayed in Fig. 7, for $S = 3, 4, 5$. It is seen that unstable

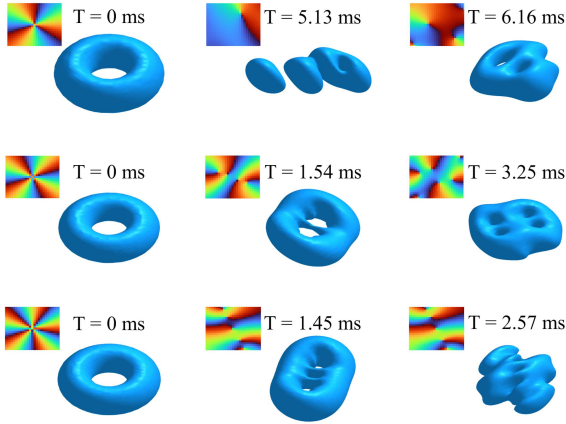


FIG. 7. The unstable evolution of perturbed vortices for $S = 3$ (first row), $S = 4$ (second row), and $S = 5$ (third row) is shown, at various times, for parameters $a_s = 100a_0$, $I = 100 \text{ MW/cm}^2$ and $\mathcal{N} = 60000$ for $S = 3$, $\mathcal{N} = 200000$ for $S = 4$, $\mathcal{N} = 220000$ for $S = 5$.

vortices fail to maintain their topological structure in the course of the evolution, eventually decaying into GS.

V. DYNAMICS

A. Orbiting bound states

The next objective is to study two-TSTM dynamics in the model. In this direction, we have found that two GSs, as well as two vortices, with identical or opposite topological charges alike, can also stably rotate around bound states. The dynamics is quite similar for the mutually orbiting GSs or vortices. In Fig. 8, we address the rotating bound states of two vortices with $S_{1,2} = \pm 1$ (the case of $S_1 = S_2 = 1$ seems nearly the same). The corresponding initial states were taken as

$$\begin{aligned} \phi(x, y, z, t = 0) = & \varphi_1(x, y - y_0, z, t = 0)e^{-i\eta x} \\ & + \varphi_2(x, y + y_0, z, t = 0)e^{i\eta x}, \end{aligned} \quad (30)$$

where $\varphi_1(x, y - y_0, z)$ is the vortex with $S = 1$, initially centered at $y = -y_0$, and $\varphi_2(x, y + y_0, z)$ is the vortex with $S = -1$ initially located at $y = y_0$. It is necessary to choose y_0 large enough, so that the two vortices are initially placed far from each other, avoiding overlap. To set the pair in rotation, kicks of equal magnitudes are applied to the upper and lower vortices in the negative and positive x -direction, respectively. In Fig. 8(a)-(f), we display the rotating bound states of the vortex-antivortex pair at different times. The figure shows that, in the course of the presented time interval, the two vortices rotate around each other by an angle close to 180° . Although the distance between them somewhat varies during the rotation, the bound state remains

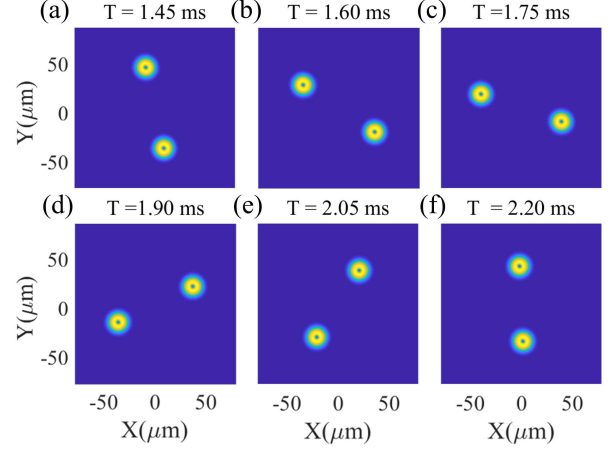


FIG. 8. The stable rotation of the vortex-antivortex bound state ($S_{1,2} = \pm 1$), with physical parameters $a_s = 100a_0$, $I = 100 \text{ MW/cm}^2$, and $\mathcal{N} = 400000$. Panels (a)-(f) show the rotating bound state at different times.

robust. While the figure displays only a half-period of the orbiting motion, long simulations corroborate that the rotating bound state remains stable, at least, until $T = 50 \text{ ms}$.

We have also tested rotating three- and four-body bound states, concluding that they are always unstable, unlike the binary ones. In particular, a bound state of three GSs can perform no more than two rotation periods, which is followed by the merger or separation (not shown here in detail).

B. Collisions

Apart from the formation of the rotational bound states, it is also relevant to consider interaction between TSTMs in the form of head-on collisions between them. Previous studies primarily focused on the collisions between fundamental solitons (with $S = 0$), or between vortex states with $S = 1$ [95, 112–114]. In this section, we extend the investigation by examining not only the collisions between vortex TSTMs with $S = 1$, but also between ones with ($S > 1$), as well as vortex-antivortex collisions, with $S = \pm 1$.

Under the action of opposite kicks of size $\pm\eta$, two vortices demonstrate head-on collisions between the vortices moving in the x direction. The corresponding initial states were constructed as

$$\begin{aligned} \phi(x, y, z, t = 0) = & \varphi(x - x_0, y, z, t = 0)e^{-i\eta x} \\ & + \varphi(x + x_0, y, z, t = 0)e^{+i\eta x}, \end{aligned} \quad (31)$$

where $\varphi(x \pm x_0, y, z)$ represents the vortices with topological charges S_1 and S_2 initially centered at $x = \pm x_0$. Similar to the case of rotation, it is necessary to choose a

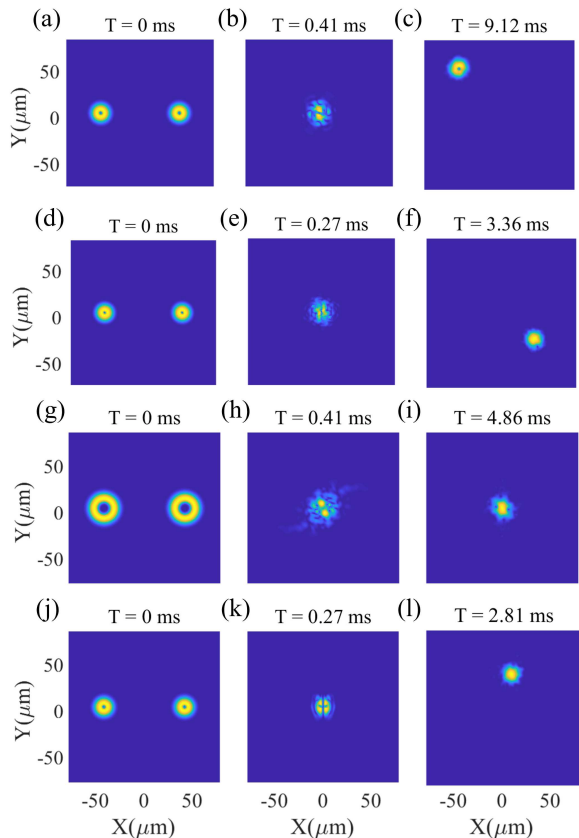


FIG. 9. Collision dynamics: $a_s = 100a_0$, $I = 100 \text{ MW/cm}^2$, $\eta = 0.1$, with $\mathcal{N} = 200000$ for $S = 1$ (a-c) and $S = -1$ (j-l); $\mathcal{N} = 375000$ for $S = 1$ (d-f); and $\mathcal{N} = 270000$ for $S = 4$ (g-i). (a-c) illustrate the collision between two $S = 1$ vortices, where (b) depicts the moment of collision, and (c) shows the formation of a single vortex moving in a specific direction after the collision. Similarly, (d-f) also present the collision of two $S = 1$ vortices; however, due to the difference in atom numbers, the outcome is a ground state that moves in a specific direction, as indicated in (f). (g-i) demonstrate the collision between two $S = 4$ vortices, characterized as a completely inelastic collision, with (i) illustrating the transition to a ground state that remains stationary at the collision point. Lastly, (j-l) depict the collision between a vortex and an antivortex with $S_1 = -S_2 = 1$; (k) represents the moment of collision, while (l) shows the synthesis of a ground state that moves in a specific direction following the collision.

sufficiently large x_0 to prevent overlap between the vortices at $t = 0$.

Fig. 9 displays the collisions between two vortices with $\eta = 0.1$ and $S_1 = S_2 = 1$, $S_1 = S_4 = 4$ and $S_1 = -S_2 = 1$ in (a)-(f), (g)-(i), and (j)-(l), respectively. The difference between Fig. 9(a-c) and (d-f) is that in the former case they represent the collision between the vortices with $S = 1$ and $\mathcal{N} = 200000$, while in the latter case the norm is essentially larger, $\mathcal{N} = 375000$. In both cases, the collisions are completely inelastic, with the difference that

the “lighter” vortices merge into a single one with the same topological charge, $S = 1$, while the “heavier” vortices merge into a GS soliton with $S = 0$. In either case, the emerging fused soliton move in some direction (actually, a random one, which is different in different realizations). Essentially the same outcomes are produced by simulations of the collisions with the higher odd value of $S_1 = S_2 = 3$. On the other hand, collisions between the vortices carrying even values of S , such as $S_{1,2} = 4$, displayed in Figs. 9(g)-(i), leads to the merger into a single GS soliton (with $S = 0$), which remains quiescent thereafter.

In Fig. 9(j)-(l), the outcome of the vortex-antivortex collision, with $S_{1,2} = \pm 1$, is quite natural, *viz.*, the merger into a GS soliton. Somewhat similar to the collision between the vortices with $S_{1,2} = 1$, which is shown in Fig. 9(d)-(f), the emerging fused GS soliton is moving aside.

Note that in Fig. 9 the total angular momentum of the interacting vortices is conserved in the collisions shown in panels (a-c) and (j-l), while it is not conserved in the cases represented by panels (d-f) and (g-i). The reason for the apparent non-conservation of the angular momentum in the latter case is that, in the course of collision, a considerable part of the angular momentum is radiated away with small-amplitude waves, and eventually lost while hitting edges of the integration domain.

The inelastic collisions are produced by the slow collisions, with relatively small values of kick η . On the other hand, fast collisions, initiated by large values of η , are quasi-elastic, i.e., the colliding solitons pass through each other. Such results were demonstrated in simulations performed for fast collisions between vortex solitons with $S_{1,2} = 1$ in the framework of the 3D SP system in Ref. [95]. A threshold value of η , which a boundary between the elastic and inelastic collisions, is significantly affected by the atom number \mathcal{N} and topological charge S . In particular, for $S = 1$ and $\mathcal{N} = 80000$, the threshold corresponds to $\eta \approx 1$.

To conclude this section, it is relevant to mention that simulations of collisions between genuine compactons performed in the framework of the respective real nonlinear equations, reveal creation of small-amplitude compacton-anticompacton pairs [26]. No similar effect is produced by the present system, which stresses its difference from those which give rise to genuine compactons.

VI. CONCLUSION

We have investigated self-trapped states in BEC with the gravity-like $(-1/r)$ long-range interatomic interaction, that can be induced by the laser illumination of the condensate. The system is described by the 3D GPE (Gross-Pitaevskii equation), which belong to the class of SP (Schrödinger-Poisson) models. Using the VA (variational approximation) and systematically collected numerical results, we have found that the GPE

gives rise to the three-dimensional TSTMs (tightly self-trapped modes). The VA, based on a compacton ansatz, produces results which are very close to their numerical counterparts, while the Gaussian ansatz produces less accurate predictions. The analytical solution for the decaying tails of the self-trapped states explains the sharp edges featured by TSTMs. It is also found that the self-trapping takes place above a threshold value of the norm. Real-time evolution demonstrates that under the influence of the $-1/R$ nonlocal interaction, TSTMs can spontaneously emerge from a loosely bound state. This finding highlights that the long-range gravity-like interaction plays a key role in both the formation and stabilization of the tightly bound state. In addition to the GS (ground state), the system supports stable TSTMs with embedded vorticity, which feature the 3D toroidal structure, with topological charges up to $S = 6$. Pairs of GSs, as well as vortex-vortex and vortex-antivortex ones, give rise to stable rotating bound states. Head-on collisions of the two vortices under small kick produce completely inelastic outcomes, *viz.*, merger into a GS soliton that stays stationary at the collision point or drifts aside, or the merger into a vortex state that also moves aside.

As an extension of the current work, it may be interesting to add the Lee-Huang-Yang (LHY) correction term to the underlying GPE, and explore formation of self-trapped quantum droplets in the system, cf. Refs. [115, 116]. A key feature of the quantum droplets is their flat-top structure, resulting from the balance between the cubic (mean-field) and LHY nonlinear terms [117–119]. In particular, one may expect the existence of QCs with the flat-top intrinsic structure.

ACKNOWLEDGMENTS

This work was supported by NNSFC (China) through Grants No. 12274077, 12475014, 11874112, 11905032, the Natural Science Foundation of Guangdong province through Grant No. 2025A1515011128, 2024A1515030131, 2023A1515010770, the Research Fund of Guangdong-Hong Kong-Macao Joint Laboratory for Intelligent Micro-Nano Optoelectronic Technology through grant No.2020B1212030010. The work of B.A.M. is supported, in part, by the Israel Science Foundation through grant No. 1695/2022.

-
- [1] N. J. Zabuski and M. D. Kruskal, Interaction of “Solitons” in a Collisionless Plasma and the Recurrence of Initial States, *Phys. Rev. Lett.* **15**, 240 (1965).
 - [2] V. E. Zakharov and A. B. Shabat, Exact Theory of Two-dimensional Self-focusing and One-dimensional Self-modulation of Waves in Nonlinear Media, *Zh. Eksp. Teor. Fiz.* **61**, 118-134 (1971) [English translation: *J. Exp. Theor. Phys.* **34**, 62-69 (1972)].
 - [3] V. E. Zakharov, S. V. Manakov, S. P. Novikov, and L. P. Pitaevskii, *Theory of Solitons: The Inverse Problem Method* (Nauka Publishers, Moscow, 1980) (English translation: Consultants Bureau, New York, 1984).
 - [4] M. J. Ablowitz and H. Segur, *Solitons and the Inverse Scattering Transform* (SIAM, Philadelphia, 1981).
 - [5] A. Newell, *Solitons in Mathematics and Physics* (SIAM, Philadelphia, 1985).
 - [6] P. G. Drazin and R. S. Johnson, *Solitons: An Introduction*, 2nd ed. (Cambridge University Press, Cambridge, 1989).
 - [7] A. C. Scott, F. Y. F. Chu, and D. W. McLaughlin, The soliton: A new concept in applied science, *Proceedings of the IEEE* **61**, 1443 (1973).
 - [8] R. Friedberg, T. D. Lee, and A. Sirlin, Class of scalar-field soliton solutions in three space dimensions, *Phys. Rev. D* **13**, 2739 (1976).
 - [9] R. Hirota and J. Satsuma, Soliton solutions of a coupled Korteweg-de Vries equation, *Phys. Lett. A* **85**, 407 (1981).
 - [10] R. Hirota, Soliton Solutions to the BKP Equations. I. the Pfaffian technique, *J. Phys. Soc. Jpn.* **58**, 2285 (1989).
 - [11] Y. S. Kivshar and B. A. Malomed, Dynamics of solitons in nearly integrable systems, *Rev. Mod. Phys.* **61**, 763 (1989).
 - [12] F. Abdullaev, S. Darmanyan, and P. Khabibullaev, *Optical Solitons* (Springer-Verlag, Berlin, 1993).
 - [13] P. D. Drummond, K. V. Kheruntsyan, and H. He, Coherent Molecular Solitons in Bose-Einstein Condensates, *Phys. Rev. Lett.* **81**, 3055 (1998).
 - [14] L. F. Mollenauer, R. H. Stolen, and J. P. Gordon, Experimental Observation of Picosecond Pulse Narrowing and Solitons in Optical Fibers, *Phys. Rev. Lett.* **45**, 1095-1098 (1980).
 - [15] V. N. Serkin and A. Hasegawa, Novel Soliton Solutions of the Nonlinear Schrödinger Equation Model, *Phys. Rev. Lett.* **85**, 4502 (2000).
 - [16] K. E. Strecker, G. B. Partridge, A. G. Truscott, and R. G. Hulet, Formation and propagation of matter-wave soliton trains, *Nature* **417**, 150-153 (2002).
 - [17] L. Khaykovich, F. Schreck, G. Ferrari, T. Bourdel, J. Cubizolles, L. D. Carr, Y. Castin, and C. Salomon, Formation of a Matter-Wave Bright Soliton, *Science* **296**, 1290-1293 (2002).
 - [18] M. A. Helal, Soliton solution of some nonlinear partial differential equations and its applications in fluid mechanics, *Chaos, Solitons & Fractals* **13**, 1917 (2002).
 - [19] Y. S. Kivshar and G. P. Agrawal, *Optical Solitons: From Fibers to Photonic Crystals* (Academic Press, San Diego, 2003).
 - [20] Dauxois T. and M. Peyrard, *Physics of Solitons* (Cambridge University Press, Cambridge, 2006)
 - [21] P. G. Kevrekidis and D. J. Frantzeskakis, *Solitons in Coupled Nonlinear Schrödinger Models: A Survey of Recent Developments*, *Rev. Phys.* **1**, 140 (2016).
 - [22] Z.-Z. Si, D.-L. Wang, B.-W. Zhu, Z.-T. Ju, X.-P. Wang, W. Liu, B. A. Malomed, Y.-Y. Wang, and C.-Q. Dai, Deep Learning for Dynamic Modeling and Coded Information Storage of Vector-Soliton Pulsations in Mode-

- Locked Fiber Lasers, *Laser Photonics Rev.* **18**, 2400097 (2024).
- [23] Z.-Z. Si, Y.-Y. Wang, and C.-Q. Dai, Switching, explosion, and chaos of multi-wavelength soliton states in ultrafast fiber lasers, *SCPMA* **67**, (2024).
- [24] L. Zeng, B. A. Malomed, D. Mihalache, J. Li, and X. Zhu, Solitons in composite linear-nonlinear moiré lattices, *Opt. Lett.*, **49**, 6944 (2024).
- [25] B. A. Malomed, *Multidimensional Solitons* (AIP Publishing, Melville, NY, 2022).
- [26] P. Rosenau and J. M. Hyman, Compactons: Solitons with finite wavelength, *Phys. Rev. Lett.* **70**, 564 (1993).
- [27] P. Rosenau, and A. Zilburg, Compactons, *J. Phys. A: Math. Theor.* **51**, 343001 (2018).
- [28] Y. S. Kivshar, Intrinsic localized modes as solitons with a compact support, *Phys. Rev. E* **48**, R43-R45 (1993).
- [29] J. E. Prilepsky, A. S. Kovalev, and Y. S. Kivshar, Magnetic polarons in one-dimensional antiferromagnetic chains, *Phys. Rev. B* **74**, 132404 (2005).
- [30] F. Kh. Abdullaev, P. G. Kevrekidis and M. Salerno, Compactons in nonlinear Schrödinger lattices with strong nonlinearity management, *Phys. Rev. Lett.* **105**, 113901 (2010).
- [31] L. Santos, G. V. Shlyapnikov, P. Zoller, and M. Lewenstein, Bose-Einstein Condensation in Trapped Dipolar Gases, *Phys. Rev. Lett.* **85**, 1791 (2000).
- [32] K. Góral, K. Rzazewski, and T. Pfau, Bose-Einstein Condensation with Magnetic Dipole-Dipole Forces, *Phys. Rev. A* **61**, 051601 (2000).
- [33] U. R. Fischer, Stability of quasi-two-dimensional Bose-Einstein condensates with dominant dipole-dipole interactions, *Phys. Rev. A* **73**, 031602 (2006).
- [34] M. A. Baranov, Theoretical Progress in Many-Body Physics with Ultracold Dipolar Gases, *Phys. Rep.* **464**, 71 (2008).
- [35] I. Tikhonenkov, B. A. Malomed, and A. Vardi. Anisotropic solitons in dipolar Bose-Einstein condensates. *Phys. Rev. Lett.* **100**, 090406 (2008).
- [36] T. Lahaye, C. Menotti, L. Santos, M. Lewenstein, and T. Pfau, The physics of dipolar bosonic quantum gases, *Rep. Prog. Phys.* **72**, 126401 (2009).
- [37] L. Chomaz, I. Ferrier-Barbut, F. Ferlaino, B. Laburthe-Tolra, B. L. Lev, and T. Pfau, Dipolar physics: a review of experiments with magnetic quantum gases, *Rep. Prog. Phys.* **86**, 026401 (2022).
- [38] N. Defenu, T. Donner, T. Macrì, G. Pagano, S. Ruffo, and A. Trombettoni, Long-range interacting quantum systems, *Rev. Mod. Phys.* **95**, 035002 (2023).
- [39] N. Bigagli, W. Yuan, S. Zhang, B. Bulatovic, T. Karman, I. Stevenson, and S. Will, Observation of Bose-Einstein Condensation of Dipolar Molecules, *Nature* **631**, 289 (2024).
- [40] A. K. Mohapatra, T. R. Jackson, and C. S. Adams, Coherent Optical Detection of Highly Excited Rydberg States Using Electromagnetically Induced Transparency, *Phys. Rev. Lett.* **98**, 113003 (2007).
- [41] T. A. Johnson, E. Urban, T. Henage, L. Isenhower, D. D. Yavuz, T. G. Walker, and M. Saffman, Rabi Oscillations between Ground and Rydberg States with Dipole-Dipole Atomic Interactions, *Phys. Rev. Lett.* **100**, 113003 (2008).
- [42] R. Heidemann, U. Krohn, V. Bendkowsky, B. Butscher, R. Löw, and T. Pfau, Rydberg Excitation of Bose-Einstein Condensates, *Phys. Rev. Lett.* **100**, 033601 (2008).
- [43] M. Saffman, T. G. Walker, and K. Mølmer, Quantum information with Rydberg atoms, *Rev. Mod. Phys.* **82**, 2313 (2010).
- [44] J. B. Balewski, A. T. Krupp, A. Gaj, S. Hofferberth, R. Löw, and T. Pfau, Rydberg dressing: understanding of collective many-body effects and implications for experiments, *New J. Phys.* **16**, 063012 (2014).
- [45] Y.-C. Zhang, V. Walther, and T. Pohl, Long-Range Interactions and Symmetry Breaking in Quantum Gases through Optical Feedback, *Phys. Rev. Lett.* **121**, 073604 (2018).
- [46] G. Li, X. Jiang, B. Liu, Z. Chen, B. A. Malomed, and Y. Li, Two-dimensional anisotropic vortex quantum droplets in dipolar Bose-Einstein condensates, *Front. Phys.* **19**, 22202 (2024).
- [47] Y.-C. Zhang, T. Pohl, and F. Maucher, Phases of supersolids in confined dipolar Bose-Einstein condensates, *Phys. Rev. A* **104**, 013310 (2021).
- [48] L.-J. He, B. Liu, and Y.-C. Zhang, Quantum droplets in dipolar condensate mixtures with arbitrary dipole orientations, *Phys. Rev. A* **110**, 013308 (2024).
- [49] A. Yang, J. Zhou, X. Liang, G. Li, B. Liu, H.-B. Luo, B. A. Malomed, and Y. Li, Two-dimensional quantum droplets in binary quadrupolar condensates, *New J. Phys.* **26**, 053037 (2024).
- [50] Y.-C. Zhang, F. Maucher, and T. Pohl, Supersolidity around a Critical Point in Dipolar Bose-Einstein Condensates, *Phys. Rev. Lett.* **123**, 015301 (2019).
- [51] Y. Chen, Z. Bai, C. Hang, and G. Huang, Giant nonlocal Kerr nonlinearity and polaritonic solitons in a Rydberg-dressed Bose-Einstein condensate, *Opt. Express*, **31**, 33518 (2023).
- [52] G. Li, Z. Zhao, X. Jiang, Z. Chen, B. Liu, B. A. Malomed, and Y. Li, Strongly Anisotropic Vortices in Dipolar Quantum Droplets, *Phys. Rev. Lett.* **133**, 053804 (2024).
- [53] H. Zhu, Y.-Q. Ma, W.-K. Bai, Y.-M. Yu, F.-F. Ye, Y.-Y. Li, L. Zhuang, and W.-M. Liu, Three-dimensional isotropic droplets in Rydberg-dressed Bose gases, *Phys. Rev. Res.* **6**, 023151 (2024).
- [54] D. O'Dell, S. Giovanazzi, G. Kurizki and V. M. Akulin, Bose-Einstein condensates with $\frac{1}{r}$ interatomic attraction: Electromagnetically induced “gravity”, *Phys. Rev. Lett.* **84**, 5687 (2000).
- [55] I. Papadopoulos, P. Wagner, G. Wunner, and J. Main, Bose-Einstein condensates with attractive $1/r$ interaction: The case of self-trapping, *Phys. Rev. A* **76**, 053604 (2007).
- [56] P. M. Lushnikov, Collapse and stable self-trapping for Bose-Einstein condensates with $1/r^b$ -type attractive interatomic interaction potential, *Phys. Rev. A* **82**, 023615 (2010).
- [57] F. Maucher, S. Skupin, M. Shen, and W. Krolikowski, Rotating three-dimensional solitons in Bose-Einstein condensates with gravitylike attractive nonlocal interaction, *Phys. Rev. A* **81**, 063617 (2010).
- [58] K. Pal and U. R. Fischer, Quantum nonlinear effects in the number-conserving analog gravity of Bose-Einstein condensates, *Phys. Rev. D* **110**, 116022 (2024).
- [59] S. Rau, J. Main, and G. Wunner, Variational methods with coupled Gaussian functions for Bose-Einstein condensates with long-range interactions. I. General concept, *Phys. Rev. A* **82**, 023610 (2010).

- [60] S. Rau, J. Main, H. Cartarius, P. Köberle, and G. Wunner, Variational methods with coupled Gaussian functions for Bose-Einstein condensates with long-range interactions. II. Applications, *Phys. Rev. A* **82**, 023611 (2010).
- [61] Y. V. Kartashov, G. E. Astrakharchik, B. A. Malomed, and L. Torner, Frontiers in multidimensional self-trapping of nonlinear fields and matter, *Nat. Rev. Phys.* **1**, 185 (2019).
- [62] M. L. Quiroga-Teixeiro, A. Berntson, and H. Michinel, Internal dynamics of nonlinear beams in their ground states: short- and long-lived excitation, *J. Opt. Soc. Am. B* **16**, 1697 (1999).
- [63] I. Towers, A. V. Buryak, R. A. Sammut, B. A. Malomed, L.-C. Crasovan, and D. Mihalache, Stability of spinning ring solitons of the cubic-quintic nonlinear Schrödinger equation, *Phys. Lett. A* **288**, 292 (2001).
- [64] M. Quiroga-Teixeiro and H. Michinel, Stable azimuthal stationary state in quintic nonlinear optical media, *J. Opt. Soc. Am. B* **14**, 2004 (1997).
- [65] A. Desyatnikov, A. Maimistov, and B. Malomed, Three-dimensional spinning solitons in dispersive media with the cubic-quintic nonlinearity, *Phys. Rev. E* **61**, 3107 (2000).
- [66] D. Mihalache, D. Mazilu, L.-C. Crasovan, I. Towers, A. V. Buryak, B. A. Malomed, L. Torner, J. P. Torres, and F. Lederer, Stable spinning optical solitons in three dimensions, *Phys. Rev. Lett.* **88**, 073902 (2002).
- [67] H. Sakaguchi, B. Li, and B. A. Malomed, Creation of two-dimensional composite solitons in spin-orbit-coupled self-attractive Bose-Einstein condensates in free space, *Phys. Rev. E* **89**, 032920 (2014).
- [68] Y.-C. Zhang, Z.-W. Zhou, B. A. Malomed, and H. Pu, Stable solitons in three dimensional free space without the ground state: Self-trapped Bose-Einstein condensates with spin-orbit coupling, *Phys. Rev. Lett.* **115**, 253902 (2015).
- [69] L. Dong, Y. V. Kartashov, L. Torner, and A. Ferrando, Vortex Solitons in Twisted Circular Waveguide Arrays, *Phys. Rev. Lett.* **129**, 123903 (2022).
- [70] H. Zhang, M. Chen, L. Yang, B. Tian, C. Chen, Q. Guo, Q. Shou, and W. Hu, Higher-charge vortex solitons and vector vortex solitons in strongly nonlocal media, *Opt. Lett.*, **44**, 3098 (2019).
- [71] D. Liu, Y. Gao, D. Fan, and L. Zhang, Higher-charged vortex solitons in harmonic potential, *Chaos, Solitons & Fractals* **171**, 113422 (2023).
- [72] L. Dong and M. Fan, Stable higher-charge vortex droplets governed by quantum fluctuations in three dimensions, *Chaos, Solitons & Fractals* **173**, 113728 (2023).
- [73] H. Zhang, T. Zhou, and C. Dai, Stabilization of higher-order vortex solitons by means of nonlocal nonlinearity, *Phys. Rev. A* **105**, 013520 (2022).
- [74] L. Dong, M. Fan, and B. A. Malomed, Stable higher-charge vortex solitons in the cubic-quintic medium with a ring potential, *Opt. Lett.* **48**, 4817 (2023).
- [75] C. Li and Y. V. Kartashov, Stable Vortex Solitons Sustained by self-trapping Gain in a Cubic Medium, *Phys. Rev. Lett.* **132**, 213802 (2024).
- [76] Y. Wang, J. Cui, H. Zhang, Y. Zhao, S. Xu, and Q. Zhou, Rydberg-Induced Topological Solitons in Three-Dimensional Rotation Spin-Orbit-Coupled Bose-Einstein Condensates, *Chinese Phys. Lett.* **41**, 090302 (2024).
- [77] S.-L. Xu, T. Wu, H.-J. Hu, J.-R. He, Y. Zhao, and Z. Fan, Vortex solitons in Rydberg-excited Bose-Einstein condensates with rotating PT-symmetric azimuthal potentials, *Chaos, Solitons & Fractals* **184**, 115043 (2024).
- [78] A. Navarrete, A. Paredes, J. R. Salgueiro, and H. Michinel, Spatial solitons in thermo-optical media from the nonlinear Schrödinger-Poisson equation and dark-matter analogs, *Phys. Rev. A* **95**, 013844 (2017).
- [79] I. M. Moroz, R. Penrose, and P. Tod, Spherically-symmetric solutions of the Schrödinger-Newton equations, *Classical and Quantum Gravity* **15**, 2733–2742 (1998).
- [80] D. Ruiz, The Schrödinger-Poisson equation under the effect of a nonlinear local term, *J. Functional Analysis* **237**, 655–674 (2006).
- [81] B. Schwabe, J. C. Niemeyer, and J. F. Engels, Simulations of solitonic core mergers in ultralight axion dark matter cosmologies, *Phys. Rev. D* **94**, 043513 (2016).
- [82] L. Hui, J. P. Ostriker, S. Tremaine, and E. Witten, Ultralight scalars as cosmological dark matter, *Phys. Rev. D* **95**, 043541 (2017).
- [83] H.-Y. Schive, T. Chiueh, and T. Broadhurst, Cosmic structure as the quantum interference of a coherent dark wave, *Nature Phys.* **10**, 496 (2014).
- [84] L. Hui, Wave Dark Matter, *Annu. Rev. Astron. Astrophys.* **59**, 247 (2021).
- [85] L. Zhao and F. Zhao, On the existence of solutions for the Schrödinger-Poisson equations, *J. Math. Anal. Appl.* **346**, 155–169 (2008).
- [86] A. Ambrosetti, On Schrödinger-Poisson systems, *Milan J. Mathematics* **76**, 257–274 (2008).
- [87] R. Ruffini, Systems of Self-Gravitating Particles in General Relativity and the Concept of an Equation of State, *Phys. Rev.* **187**, 1767 (1969).
- [88] P.-H. Chavanis, Mass-radius relation of Newtonian self-gravitating Bose-Einstein condensates with short-range interactions. I. Analytical results, *Phys. Rev. D* **84**, 043531 (2011).
- [89] P.-H. Chavanis and L. Delfini, Mass-radius relation of Newtonian self-gravitating Bose-Einstein condensates with short-range interactions. II. Numerical results, *Phys. Rev. D* **84**, 043532 (2011).
- [90] B. Eliasson and P. K. Shukla, Formation and dynamics of coherent structures involving phase-space vortices in plasmas, *Phys. Rep.* **422**, 225–290 (2006).
- [91] K. Asakawa and M. Tsubota, Corotation of two quantized vortices coupled with collective modes in self-gravitating Bose-Einstein condensates, *Phys. Rev. A* **110**, 053310 (2024).
- [92] Y. O. Nikolaieva, A. O. Olashyn, Y. I. Kuriatnikov, S. I. Vilchynskii, and A. I. Yakimenko, Stable vortex in Bose-Einstein condensate dark matter, *Low Temp. Phys.* **47**, 684 (2021).
- [93] A. Paredes, D. N. Olivieri, and H. Michinel, From optics to dark matter: A review on nonlinear Schrödinger-Poisson systems, *Physica D* **403**, 132302 (2020).
- [94] V. M. Lashkin, O. K. Cheremnykh, Z. Ehsan, and N. Batool, Three-dimensional vortex dipole solitons in self-gravitating systems, *Phys. Rev. E* **107**, 024201 (2023).
- [95] Y. O. Nikolaieva, Y. M. Bidasyuk, K. Korshynska, E. V. Gorbar, J. Jia, and A. I. Yakimenko, Stable vortex structures in colliding self-gravitating Bose-Einstein condensates, *Phys. Rev. D* **108**, 023503 (2023).

- [96] A. S. Dmitriev, D. G. Levkov, A. G. Panin, E. K. Pushnaya, and I. I. Tkachev, Instability of rotating Bose stars, *Phys. Rev. D* **104**, 023504 (2021).
- [97] Y. O. Nikolaieva, A. O. Olashyn, Y. I. Kuriatnikov, S. I. Vilchynskii, and A. I. Yakimenko, Stable vortex in Bose-Einstein condensate dark matter, *Low Temp. Phys.* **47**, 684 (2021).
- [98] J. Garnier, K. Baudin, A. Fusaro, and A. Picozzi, Incoherent localized structures and hidden coherent solitons from the gravitational instability of the Schrödinger-Poisson equation, *Phys. Rev. E* **104**, 054205 (2021).
- [99] J. Yang, *Nonlinear Waves in Integrable and Non-Integrable Systems* (SIAM, Philadelphia, 2010).
- [100] J. Yang, Newton-conjugate-gradient methods for solitary wave computations, *J. Comput. Phys.* **228**, 7007 (2009).
- [101] B. Liu, Y. X. Chen, A. W. Yang, X. Y. Cai, Y. Liu, Z. H. Luo, X. Z. Qin, X. D. Jiang, Y. Y. Li, and B. A. Malomed, Vortex-ring quantum droplets in a radially-periodic potential, *New J. Phys.* **24**, 123026 (2022).
- [102] Y. Li, Z. Chen, Z. Luo, C. Huang, H. Tan, W. Pang, and B. A. Malomed, Two-Dimensional Vortex Quantum Droplets, *Phys. Rev. A* **98**, 063602 (2018).
- [103] C. Huang, L. Lyu, H. Huang, Z. Chen, S. Fu, H. Tan, B. A. Malomed, and Y. Li, Dipolar bright solitons and solitary vortices in a radial lattice, *Phys. Rev. A* **96**, 053617 (2017).
- [104] C. Huang, Excited states of two-dimensional solitons supported by spin-orbit coupling and field-induced dipole-dipole repulsion, *Phys. Rev. A* **97**, 013636 (2018).
- [105] R.-X. Zhong, Z.-P. Chen, C.-Q. Huang, Z.-H. Luo, H.-S. Tan, B. A. Malomed, and Y.-Y. Li, Self-trapping under two-dimensional spin-orbit coupling and spatially growing repulsive nonlinearity, *Front. Phys.* **13**, 130311 (2018).
- [106] L. Dong, M. Fan, and B. A. Malomed, Stable higher-order vortex quantum droplets in an annular potential, *Chaos, Solitons & Fractals* **179**, 114472 (2024).
- [107] X. Xu, F. Zhao, Y. Zhou, B. Liu, X. Jiang, B. A. Malomed, and Y. Li, Vortex gap solitons in spin-orbit coupled Bose-Einstein condensates with competing nonlinearities, *Commun. Nonlinear Sci. Numer. Simul.* **117**, 106930 (2023).
- [108] Z. Zhao, G. Chen, B. Liu, and Y. Li, Discrete vortex quantum droplets, *Chaos, Solitons & Fractals* **162**, 112481 (2022).
- [109] X. Chen, Z. Zhao, X. Zheng, H. Huang, H. Wang, Y. Liu, and G. Chen, Hidden-vortex quantum droplets in an optical lattice, *Phys. Lett. A* **517**, 129654 (2024).
- [110] Y. V. Kartashov, V. A. Vysloukh, and L. Torner, Stability of vortex solitons in thermal nonlinear media with cylindrical symmetry, *Opt. Express*, **15**, 9378 (2007).
- [111] A. Paredes, J. Blanco-Labrador, D. N. Olivieri, J. R. Salgueiro, and H. Michinel, Vortex revivals and Fermi-Pasta-Ulam-Tsingou recurrence, *Phys. Rev. E* **99**, 062211 (2019).
- [112] A. Paredes and H. Michinel, Interference of dark matter solitons and galactic offsets, *Phys. Dark Universe* **12**, 50 (2016).
- [113] D.-I. Choi, Collision of gravitationally bound Bose-Einstein condensates, *Phys. Rev. A* **66**, 063609 (2002).
- [114] A. Bernal and F. S. Guzmán, Scalar field dark matter: Head-on interaction between two structures, *Phys. Rev. D* **74**, 103002 (2006).
- [115] D. S. Petrov, Quantum Mechanical Stabilization of a Collapsing Bose-Bose Mixture, *Phys. Rev. Lett.* **115**, 155302 (2015).
- [116] D. S. Petrov and G. E. Astrakharchik, Ultradilute Low-Dimensional Liquids, *Phys. Rev. Lett.* **117**, 100401 (2016).
- [117] Z.-H. Luo, W. Pang, B. Liu, Y.-Y. Li, and B. A. Malomed, A new form of liquid matter: Quantum droplets, *Front. Phys.* **16**, 32201 (2020).
- [118] M. Guo and T. Pfau, A new state of matter of quantum droplets, *Front. Phys.* **16**, 32202 (2020).
- [119] F. Böttcher, J.-N. Schmidt, J. Hertkorn, K. S. H. Ng, S. D. Graham, M. Guo, T. Langen, and T. Pfau, New states of matter with fine-tuned interactions: quantum droplets and dipolar supersolids, *Rep. Prog. Phys.* **84**, 012403 (2020).